

See discussions, stats, and author profiles for this publication at: <https://www.researchgate.net/publication/51050255>

Molecular Orientation of Asphaltenes and PAH Model Compounds in Langmuir–Blodgett Films Using Sum Frequency Generation Spectroscopy

ARTICLE in LANGMUIR · MAY 2011

Impact Factor: 4.46 · DOI: 10.1021/la200466b · Source: PubMed

CITATIONS

37

READS

24

7 AUTHORS, INCLUDING:



A. Ballard Andrews
Schlumberger Limited
67 PUBLICATIONS 1,273 CITATIONS

[SEE PROFILE](#)



Arthur McClelland
Harvard University
15 PUBLICATIONS 147 CITATIONS

[SEE PROFILE](#)



Amber Krummel
Colorado State University
23 PUBLICATIONS 641 CITATIONS

[SEE PROFILE](#)



Oliver C Mullins
Schlumberger Limited
245 PUBLICATIONS 5,976 CITATIONS

[SEE PROFILE](#)

Molecular Orientation of Asphaltenes and PAH Model Compounds in Langmuir–Blodgett Films Using Sum Frequency Generation Spectroscopy

A. Ballard Andrews,^{*†} Arthur McClelland,[‡] Oona Korkeila,^{†§} Alexander Demidov,[‡] Amber Krummel,^{||,⊥} Oliver C. Mullins,[†] and Zhan Chen[#]

[†]Schlumberger-Doll Research, Cambridge, Massachusetts, United States

[‡]Northeastern University, Boston, Massachusetts, United States

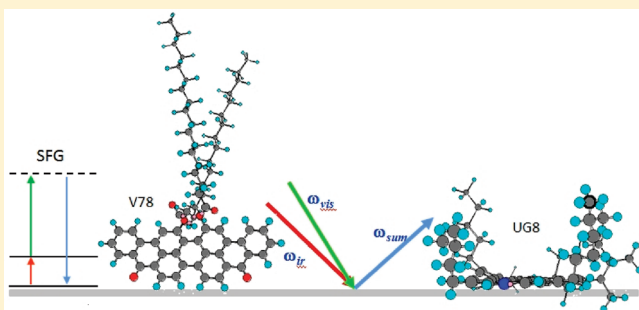
[§]Helsinki University of Technology, Helsinki, Finland

^{||}Harvard University, Cambridge, Massachusetts, United States

[⊥]Colorado State University, Fort Collins, Colorado, United States

[#]University of Michigan, Ann Arbor, Michigan, United States

ABSTRACT: Asphaltenes are an important class of compounds in crude oil whose surface activity is important for establishing reservoir rock wettability which impacts reservoir drainage. While many phenomenological interfacial studies with crude oils and asphaltenes have been reported, there is very little known about the molecular level interactions between asphaltenes and mineral surfaces. In this study, we analyze Langmuir–Blodgett films of asphaltenes and related model compounds with sum frequency generation (SFG) vibrational spectroscopy. In SFG, the polarization of the input (vis, IR) and output (SFG) beams can be varied, which allows the orientation of different functional groups at the interface to be determined. SFG clearly indicates that asphaltene polycyclic aromatic hydrocarbons (PAHs) are highly oriented in the plane of the interface and that the peripheral alkanes are transverse to the interface. In contrast, model compounds with oxygen functionality have PAHs oriented transverse to the interface. Computational quantum chemistry is used to support corresponding band assignments, enabling robust determination of functional group orientations.



1. INTRODUCTION

Recovery factors in oil fields are well-known to be rather small. For example, in many fields, only 22% of the original oil in place is recovered by current methods. Even small increases in recovery could result in vast increases in produced crude oil, for example, by enhanced oil recovery (EOR) methods.¹ In particular, in large carbonate reservoirs in the Middle East, it is well-known that rock wettability controls irreducible oil saturation in the reservoir rock; much more oil can be recovered from water wet formations. Furthermore, the wettability changes from oil wet in the oil zone to water wet in the water zone; this wettability change often occurs continuously through an extended zone of mixed wettability.² These mixed wettability zones can contain one-half of the current field reserves in giant Middle East reservoirs. Consequently, any ability to alter wettability even if only subtly could result in huge increases in oil production.

There have been many predominantly phenomenological studies establishing the interfacial activity of asphaltenes with high energy surfaces such as water.^{3–5} There have been far fewer studies that are sensitive to the molecular orientation of asphaltenes at the interface. Langmuir isotherms for asphaltene films on

water coupled with Brewster angle microscopy (BAM) have been used to imply molecular orientations of asphaltenes.^{6–9} The data has been interpreted as consistent with the asphaltenes or polycyclic aromatic hydrocarbons (PAHs) tilted at some angle with respect to the surface normal, rather than a flat-on arrangement parallel to the interface. The evidence against a flat-on geometry is based partly on the small mean molecular area (MMA) per molecule observed in the Langmuir isotherms, which can be interpreted as due to the stacking of the molecules with either a head-on or edge-on orientation at the interface.^{6–13} As noted by several authors,^{8–11} inferring the orientation from the MMA is reliable only when a monolayer is present. The formation of nanoaggregates¹⁴ in solution prior to spreading or during the compression phase provides an alternative explanation for the observed small MMA. It is evident that the asphaltene dispersion in the bulk toluene prior to evaporation, whether molecular, nanocolloidal, or cluster dispersion, has a pronounced

Received: February 3, 2011

Revised: March 18, 2011

Table 1. Names, Chemical Formulas, Molecular Weights, and Structures of the Three Compounds Examined in This Study^a

| Full Name (Abbr.) | Chemical Formula and Molecular Weight (Da) | Molecular Structure |
|---|--|---------------------|
| N-(1-hexylheptyl)-N'-(5-carboxylicpentyl)-perylene-3,4,9,10-tetracarboxylicbisimide (C5Pe) | C ₄₈ H ₅₆ N ₂ O ₆ 757 | |
| Violanthrone-78 (V-78) | C ₇₀ H ₈₄ O ₆ 1021 | |
| Asphaltene (UG-8) | 750 (average) | |

^a For the UG8 asphaltene sample, the structure is hypothetical and the MW is the average of the distribution based on the predominant evidence.

impact on the resulting Langmuir film. Consequently, possible molecular orientation of asphaltenes must be considered with regard to the initial concentration of asphaltenes in toluene.¹⁵

Studies of PAH model compounds have reached similar conclusions.^{11,12} Perylene tetracarboxylic acid derivatives (PTCDs) form stable Langmuir–Blodgett (LB) films and provide useful analogues for comparison with asphaltenes.^{10–14} In PTCDs the π orbital overlap facilitates π – π stacking with an intermolecular distance of 3.4 Å.¹³ Excimer emission and UV–vis absorption of LB films indicate a stacking formation at the water interface, and this organization is transferable to LB films.^{12–14} The MMA from Π –A isotherms is smaller than expected for a flat-on configuration, and the consensus is that these molecules must be orientated either head-on or edge-on with the PAH core tilted at an angle with respect to the surface normal. Columnar stacking has also been reported for a perylene bisimide derivative, with an average of 11 molecules per nanoaggregate at 40°C.¹³ In addition to interesting semiconductor properties and practical applications, PTCDs have many similarities with the chemical moieties found in the asphaltene fraction. Table 1 lists the full names and structures of the model compounds investigated in this study,

and Table 2 lists some of the similarities they have with asphaltenes: properties of the two model compounds are calculated directly from the molecular structure; for UG8 (column 3–6), the averages are calculated from quantitative ¹³C NMR measurements.²⁸

When attempting to determine the molecular orientation of asphaltenes at the interface, it is important to consider asphaltene molecular architecture. This topic is still being debated in the literature; nevertheless, there appears to be convergence from many different analytical methods.^{16,17} The most probable size of asphaltene PAHs is seven fused rings as given by direct molecular imaging using scanning tunneling microscopy¹⁸ and transmission electron microscopy.¹⁹ This is consistent with a comparison of asphaltene absorption and emission spectra with exhaustive molecular orbital calculations²⁰ and with molecular dynamics simulations.²¹ Time-resolved fluorescence depolarization measurements and fluorescence correlation spectroscopy showed that the diffusion constants of asphaltenes are comparable to PTCDs.^{22–24} Both ultrahigh resolution mass spectrometry and two-color photoionization mass spectrometry are consistent with a single PAH.^{25,26} In addition, electron impact unimolecular decomposition of asphaltenes also shows that island molecular

Table 2. Comparison of Selected Properties of UG8 Asphaltene and PAH Model Compounds^a

| cmpd | wt % C | H:C atomic ratio | carbon aromaticity % | carbon aliphaticity % | bridgehead aromatic carbon % | aromatic PAH size |
|------|--------|------------------|----------------------|-----------------------|------------------------------|-------------------|
| UG8 | 81.1 | 1.1 | 49.5* | 50.5* | 27.1* | 28.5* |
| CSPe | 76.2 | 1.2 | 48 | 50 | 24 | 24 |
| V-78 | 82.3 | 1.2 | 49 | 51 | 23 | 34 |

^a For UG8, entries marked with an asterisk (*) in columns 4–7 are obtained from quantitative ¹³C NMR measurements.²⁸ For the model compounds, the entries are calculated directly from the structure.

architecture dominates asphaltenes.²⁷ The SFG data herein provides a test of the asphaltene molecular architecture in that a single large PAH compound is compatible with a high degree of molecular alignment at the interface.

Sum frequency generation (SFG) vibrational spectroscopy^{29–38} is a second-order nonlinear optical technique that is inherently surface specific because of its selection rule. Under the electric dipole approximation, SFG signal intensity is proportional to the square of the second order nonlinear susceptibility $\chi^{(2)}$ of the material. This $\chi^{(2)}$ is a polar third-rank tensor, which changes sign under the inversion operation: $\chi^{(2)}(r) = -\chi^{(2)}(-r)$. For any materials with inversion symmetry, nothing will be changed under the inversion operation: $\chi^{(2)}(r) = \chi^{(2)}(-r)$. The only possible solution for the above two equations is $\chi^{(2)} = 0$. Therefore, for materials with inversion symmetry, no SFG signal is detected (under the electric dipole approximation). Most bulk materials generally do have inversion symmetry, because various functional groups in these bulk materials more or less have a random orientation distribution and thus they would not generate SFG signals. However, for molecules or functional groups on surfaces or at interfaces, because inversion symmetry is broken at the surface/interface, the equation of $\chi^{(2)}(r) = \chi^{(2)}(-r)$ is not valid anymore. Here, $\chi^{(2)}$ does not need to be zero, and SFG signals can be detected. Moreover, the SFG surface/interface sensitivity is not determined by the penetration depth of the input laser beams on the sample. Even when the input laser beams can penetrate the entire sample, only molecules on the surface or at the interface contribute to the signal due to the SFG selection rule. In summary, SFG is allowed at interfaces or surfaces where inversion symmetry is broken, but it is forbidden in bulk media where it is intact. Therefore, the bulk produces no SFG contribution, even if the interface is buried.^{33,34}

In a typical SFG experiment, a visible (ω_{VIS}) beam and a frequency tunable infrared beam (ω_{IR}) are overlapped (temporally and spatially) on the sample (a surface or an interface). Light generated at the sum of these two frequencies, $\omega_{\text{SUM}} = \omega_{\text{VIS}} + \omega_{\text{IR}}$, is collected. In an SFG spectrum, the intensity of the sum frequency signal beam is plotted as a function of the input IR wavenumber. When the frequency of the input infrared beam matches a vibrational resonance of molecules on the surface (or at the interface), the SFG signal can be enhanced. Therefore, a SFG spectrum is similar to a Fourier transform infrared (FTIR) or Raman spectrum. By selecting the polarization of the input (vis, IR) and output (SFG) beams, the orientation of different functional groups at the interface can be probed.

As mentioned, the SFG signal intensity is proportional to the square of the second order nonlinear susceptibility of the medium which can be decomposed into a nonresonant and resonant term: $\chi^{(2)} = \chi_{\text{NR}} + \chi_{\text{R}}$, where χ_{R} depends on the density of surface molecules, their orientations, and the hyper-polarizability β . The SFG intensity is described by eq 1, where A_q is the oscillator strength, ω_q is the resonant frequency, and Γ is the line width. The intensity is enhanced when ω_{IR} is in resonance with the SF-active mode, as described above. The complex term can lead to

constructive or destructive interferences in the SFG spectrum.

$$I_{\text{SFG}} \propto \left| \chi_{\text{NR}}^{(2)} + \chi_{\text{R}}^{(2)} \right|^2 = \left| \chi_{\text{NR}}^{(2)} + \sum_q \frac{A_q}{\omega_{\text{IR}} - \omega_q + i\Gamma} \right|^2 \quad (1)$$

A_q is proportional to the product of the Raman and IR transition matrix elements. Thus, SFG vibrational modes are active only if they are both IR and Raman active. The SSP ($S_{\text{SFG}}S_{\text{vis}}P_{\text{IR}}$) polarization combination probes surface vibrational modes with a projection dipole moment perpendicular to the interface. A maximum is achieved when every molecule is aligned with its vibrational dipole component directed along the surface. The SPS polarization combination accesses modes that have transition dipole components parallel to the surface. If polarization is neglected, the SFG response can be approximated as a product of the IR and Raman intensities, which is useful for interpreting the SFG spectra.

2. METHODS

The full names, molecular structures, and MWs of the model compounds investigated in the present study are listed in Table 1. Violanthrone-78 (V-78) was dissolved in toluene from powdered samples (Sigma-Aldrich). The perylene derivative *N*-(1-hexylheptyl)-*N'*-(5-carboxylic-pentyl)-perylene-3,4,9,10-tetracarboxylicbisimide (CSPe) was synthesized and purified according to methods detailed by Nordgard et al. (ref 10 and references therein). Asphaltenes were extracted from a black oil (UG-8) using standard procedures. Briefly, an oil sample was diluted 1:40 in n-heptane and stirred for 24 h. Asphaltenes were extracted from the solution by vacuum filtration through a nylon filter with 1.2 μm pores and were washed with additional n-heptane until the wash solvent was colorless. Note that asphaltene floc sizes range from 1 to 400 μm ; consequently, they will not pass through a 1.2 μm filter (by Abram's rule). The extracted asphaltenes were then resuspended in a small volume of toluene. This solution was diluted 1:40 in n-heptane, and the asphaltenes were extracted as before. Finally, the asphaltenes were washed by extensive Soxhlet extraction in n-heptane. All samples were dissolved in spectrophotometric grade toluene.

Surface pressure-area isotherms were recorded using a KSV Instruments Teflon mini-trough (225 mm²) equipped with double Delrin barriers and a platinum Wilhelmy plate. All experiments were conducted at room temperature at a neutral pH. Before each use, the trough assembly was cleaned with toluene and ethanol, and then rinsed with ultrapure water. The pressure of the clean subphase at full compression was typically less than 0.1 mN/m. The MMA per molecule was calculated by extrapolation from the slope of the isotherm in the solid phase. To prepare Langmuir-Blodgett films,^{39–42} the KSV mini-trough was equipped with a dipping arm with a feedback system that adjusts the barriers during deposition so that the surface concentration remains constant. Target pressures for LB depositions are listed in Table 3, column 5. For preliminary film characterization, thicker films were grown on CaF₂ windows ($d = 25.38$ mm, $t = 5.59$ mm) and FTIR spectra were collected between cycles. Spreading concentrations,

Table 3. Parameters Used for Langmuir–Blodgett Film Depositions^a

| cmpd | MMA (\AA^2) | injected volume (μL) | concentration (mg/mL) | pressure (mN/m) | deposition pattern |
|------|------------------------|-----------------------------------|-----------------------|-----------------|--------------------|
| CSPe | 57 | 125 | 0.25 | 20 | Y |
| V-78 | 65 | 300 | 0.1 | 20 | Z |
| UG8 | 27 | 225 | 0.25 | 15 | Z |

^a The deposition patterns are inferred from the transfer ratios as seen in Figure 3. For the hydrophilic CaF_2 substrate, both Y and Z type are observed.

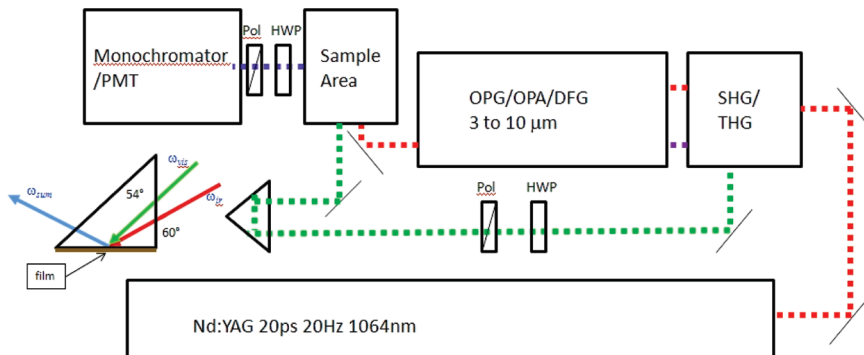


Figure 1. Experimental apparatus for SFG. A 20 Hz 20 ps Nd:YAG 1064 nm fundamental beam (red) is frequency doubled to 532 nm for the visible beam (green). Fundamental and tripled beams are sent to an OPO/OPA/DFG system to produce the tunable infrared beam from 3 to 10 μm . For a more complete description of the apparatus, see refs 30–32. Inset on the left-hand side illustrates the geometry for SFG measurements. LB films were deposited on one side of the CaF_2 prism. The 532 nm visible beam (ω_{vis}) and the tunable infrared beam (ω_{ir}) are mixed on the sample surface, and the SFG (ω_{sfg}) signal is detected.

injected volumes, surface pressures, and deposition types are listed in Table 3. The hydrophilic CaF_2 substrates were positioned below the subphase prior to spreading the solution on the surface of the subphase with a Hamilton syringe. Solvents were typically allowed to evaporate for 20–30 min before beginning to compress the barriers until the target pressure was reached. After this, we waited a further 10 min for the pressure to stabilize before beginning the deposition. Typical dipping speeds were 1–2 mm/min. After each dipping cycle, the samples were allowed to dry for at least 30 min before continuing. The transfer ratio is calculated from the decrease in area divided by the coated area of the solid substrate, $\tau = A_L/A_S$. With a hydrophilic substrate, there are two possible deposition patterns: in Y-type growth, layers are deposited head-to-head and tail-to-tail; in Z-type growth, layers are deposited head-to-tail.

FTIR spectra of the thin films and powder samples were acquired with a Bruker Vertex 70 spectrometer equipped with a Pike MIRacle attenuated total reflection (ATR) accessory. A Norton-Beer apodization function with Mertz phase correction and 4 cm^{-1} spectral resolution were employed. LB films as a function of coverage were acquired in transmission mode by removing the disk from the dipping arm holder and placing it in the FTIR sample chamber between odd numbered cycles. Long purging times (~1 h) were required to remove atmospheric CO_2 and H_2O from the sample chamber prior to scanning, and consequently, a complete series took many hours to acquire. A spectrum of the clean substrate was used as reference for each series. For background removal, we used an (iterative) rubberband procedure with 64 baseline points, which gave more consistent results than manual subtraction.

SFG spectroscopy was performed using an Eksma system (Vilnius, Lithuania) that has been described elsewhere.^{29–32} The system layout is shown in Figure 1. Briefly, the laser is operating at a 20 Hz repetition rate and generates pulses that are 20 ps in duration. The Nd:YAG 1064 nm fundamental beam was frequency doubled to 532 nm for the visible beam that was used in the SFG experiments. Fundamental and tripled beams were sent to an optical parametric oscillator/optical parametric amplifier/difference frequency generation (OPO/OPA/DFG) system to produce the tunable infrared beam from 3 to 10 μm . Thin films of

3–5 layers were deposited on CaF_2 prisms (Altos Photonics), and a near total internal reflection prism geometry was used to reduce sample damage. SFG measurements were collected by overlapping the 532 nm and tunable IR beam at incident angles of 60° and 54° to the vertical face of the prism respectively as shown in Figure 1.

For CSPe and Violanthrone we calculated the infrared and Raman spectra using the Gaussian 03 software package.⁴³ Geometry optimization was done without symmetry restrictions. Gas phase density functional theory (DFT) methods with the Lee–Yang–Parr B3LYP hybrid exchange-correlation functional^{44,45} and the 6-31G(d) basis set^{46–48} were employed. The calculations are for gas phase molecules, so there could be noticeable differences with the solid phase, but our primary motivation for performing the theoretical calculations was to identify the vibrational modes and their associated transition dipole moments (TDMs), and not to assess the accuracy of the computational model.

The product of the experimental infrared and Raman intensities should resemble the SFG intensity if polarization effects are ignored, but PAH fluorescence prevented us from obtaining the experimental Raman spectra. Therefore, we formed the product of the theoretical Raman and infrared intensities (hereafter referred to as the RIR_{th}) and compared it with the SFG. A shortcoming of this procedure is that errors in the calculated Raman spectra will affect the “predicted” SFG spectra. We applied a 20 cm^{-1} Doppler broadening to the calculated mode distributions and scaled the wavenumbers with the factor 0.9614 determined by Scott and Radom⁴⁹ for the B3LYP functional and 6-31G(d) basis set.

3. RESULTS AND DISCUSSION

The Langmuir isotherm for V-78 (Figure 2) does not exhibit a sharp liquid–solid transition, and a gradual collapse begins at 35 mN/m. The MMA of 65 \AA^2 (Table 3) is consistent with an edge-on orientation; A flat-on configuration would result in a much larger MMA (for monolayer coverage). For PTCD, the minimum intermolecular distance (IMD) is estimated to be 3.4 \AA .^{12,14} For V-78, the IMD is likely to be larger because the steric repulsion of the

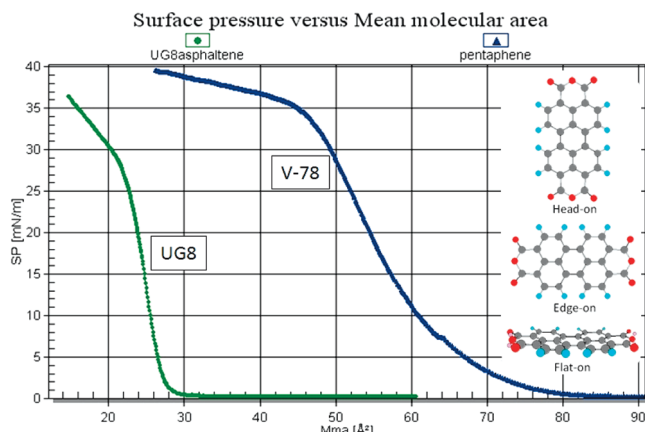


Figure 2. Langmuir isotherms for V-78 and UG8. Neither V-78 nor UG8 show a clear break in slope between the liquid and solid phases. The MMA of V-78 is smaller than that of UG8 (see Table 3 for CSPe). Inset shows three possible orientations for a PAH molecule adsorbed on the CaF_2 surface (alkyl chains not shown for clarity). In the edge-on and head-on configurations, the molecular axis could be tilted with respect to (wrt) the surface normal.

two ester groups causes a twist in the core of the PAH at the midline. A slightly larger intermolecular separation of 3.6 \AA (6%) would be sufficient to explain our observed MMA of 65 \AA^2 .

The isotherm for UG8 is also shown in Figure 2. The absence of a liquid–solid phase transition in the UG-8 isotherm has been observed by many others.^{3–11} The MMA is 27 \AA^2 (Table 3), smaller than that of V-78 or CSPe. Fluorescence correlation spectroscopy (FCS) measurements of the translational diffusion constants found that the hydrodynamic radius of V-78 and PTCDs similar to CSPe were 50% smaller on average than all petroleum derived asphaltenes.^{22–24} If asphaltenes are stacked in a head-on or even edge-on geometry, the MMA should be larger than that of CSPe or V-78. There is strong evidence in the literature^{8,9} that the asphaltenes form nanoaggregates in solution or during compression, resulting in a smaller apparent MMA.

Figure 3 shows the transfer ratios for the first few layers. For CSPe, we observed Y-type deposition (a). The two compounds without acid groups, V-78 and UG8 asphaltene, exhibited the Z-type deposition pattern (b,c). For CSPe, evidently the acid group results in the Y type because the head–head interactions are stronger than the tail–tail interactions and the molecule is able to invert during the immersion downstroke. For V-78 and UG8, the Z-type pattern indicates that there is greater conformational stability in the monolayer, and no material is deposited during immersion.

In the lower half of Figure 4, transmission FTIR spectra in the fingerprint region for three to nine cumulative layers of a CSPe LB film are displayed (dashed and solid lines). The peak intensities scale with increasing film thickness, but calibration was deemed unreliable because variations in the sample reference occurred between scans when the sample was repeatedly moved back and forth between the LB trough and the FTIR. Note that background subtraction introduces some artifacts in the LB film spectra (e.g., $1525\text{--}1475 \text{ cm}^{-1}$). The upper half of Figure 4 (solid line with markers) compares a mid-infrared (MIR) ATR spectrum from a powder sample. The powder spectrum is very similar to that of the film, except for the relative intensities of the ν_s and ν_{as} imide stretches.

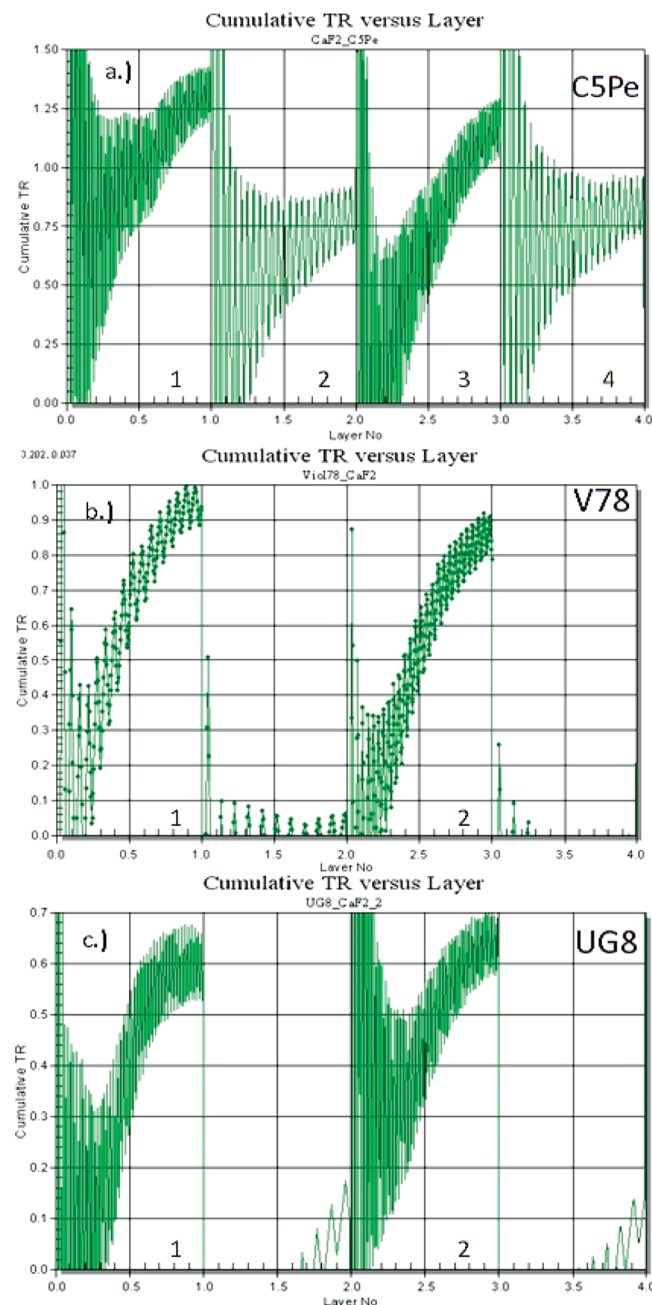


Figure 3. Cumulative transfer ratios versus layer numbers for (a) CSPe, (b) V-78, and (c) UG8. CSPe exhibits Y-type deposition (upstroke and downstroke), while V-78 and UG8 exhibit Z-type deposition (upstroke only). Spreading concentrations, injected volumes, surface pressures, and depositions patterns are listed in Table 3.

Figure 5 shows the theoretical IR (solid red) and Raman (blue dotted) calculations for V-78; the experimental FTIR-ATR is also shown (black circles). We note that the CC stretch and collective (fingerprint) modes are excited in both IR and Raman so we can anticipate that the SFG signal will also be strong for these modes. The ketone and ester both have strong IR signals but their Raman signals are small, so these modes will be weak in SFG. There is good agreement between the theoretical and experimental IR spectra for the aromatic ν_{CC} at 1580.6 cm^{-1} . The ketone mode at 1648.5 cm^{-1} is red-shifted by -16 cm^{-1} and

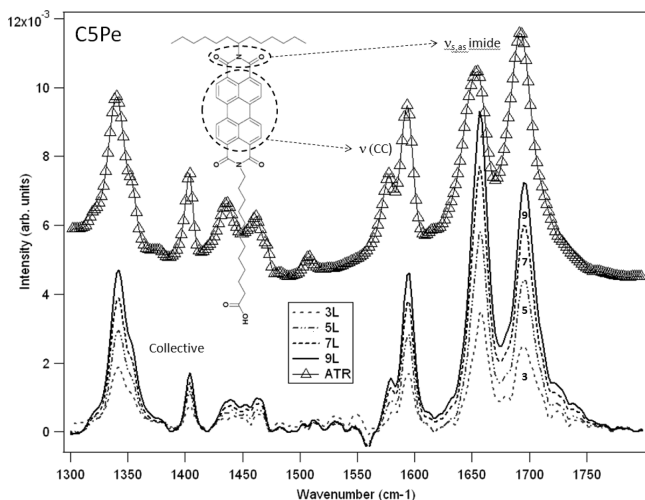


Figure 4. Lower curves show transmission FTIR spectra in the fingerprint region for three to nine cumulative layers of a C5Pe LB film on a CaF₂ substrate (dashed and solid lines). The upper curve (markers) compares a MIR-ATR spectrum from a powder sample. Note that background subtraction introduced artifacts in the LB film spectra (e.g., 1525–1475 cm⁻¹). See text for full description.

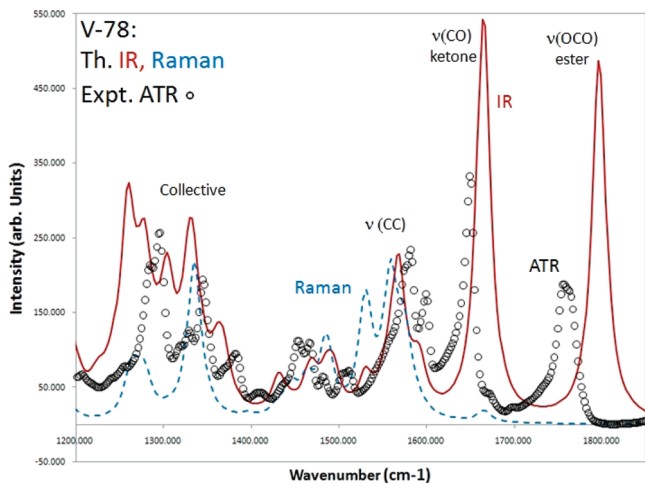


Figure 5. V-78: Theoretical calculations of IR (solid red) and Raman (blue dotted) intensities using the Gaussian software package.⁴³ The experimental FTIR-ATR is also shown (black circles). To aid comparison with the experimental spectra, the theoretical calculation has been broadened by 20 cm⁻¹ and the wavenumbers were scaled with the factor 0.9614 determined by Scott and Radom⁴⁹ for the DFT and basis set used here.

the ester at 1755.8 cm⁻¹ by a larger amount -41 cm^{-1} relative to the theory. The polar carbonyl groups would be expected to show larger spectral shifts than aromatic or alkyl (nonpolar) groups in the condensed phase because they can participate in hydrogen bonding, which is known to produce red shifts. The strongest collective ring modes at 1344.5 and 1294.3 cm⁻¹ are shifted to higher wavenumbers $+13.5 \text{ cm}^{-1}$ and $+34 \text{ cm}^{-1}$ relative to the theory. The agreement between the gas phase theoretical calculations and the condensed phase experimental data is impressive.

Figure 6 shows the theoretical calculations for C5Pe with the same conventions as in Figure 5. Similar to the V-78 molecule, the νCC stretch and collective modes are strong in both IR and Raman and

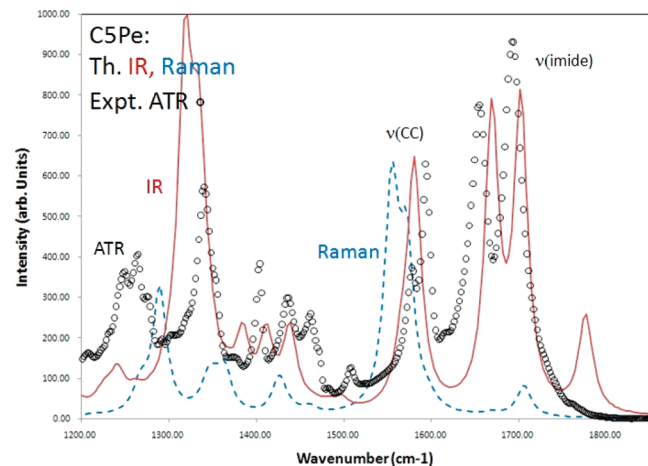


Figure 6. C5Pe: Theoretical calculations of IR (solid red) and Raman (blue dotted) intensities using the Gaussian software package.⁴³ The experimental FTIR-ATR is also shown (black circles). To aid comparison with the experimental spectra, the theoretical calculation has been broadened by 20 cm⁻¹ and the wavenumbers scaled with the factor 0.9614 determined by Scott and Radom⁴⁹ for the DFT and basis set used here.

should yield a good SFG signal. The imide and carboxylic stretches will be weak because of their small Raman strengths. The carboxylic acid is not obvious in the FTIR spectra, but there is bump on the high frequency shoulder of the ν_{as} imide mode at $\sim 1730 \text{ cm}^{-1}$ that could be attributed to COO⁻. The ν_s and ν_{as} imide modes at 1692.9 and 1653.6 cm⁻¹ are red-shifted with respect to the theory by 9 and 15.4 cm⁻¹, respectively. The aromatic νCC modes at 1593.4 and 1577.4 cm⁻¹ are blue-shifted by $\sim 10 \text{ cm}^{-1}$. A CH₂ wagging mode at 1456.8 cm⁻¹ and several collective modes at 1436.4, 1403.4, and 1339.6 cm⁻¹ are also slightly blue-shifted by -18.4 , -24.9 , -18.7 , and -5.4 cm^{-1} , respectively.

Figure 7 displays SFG spectra for a five layer V-78 LB film for SSP (top) and SPS (bottom) polarizations. The ester is not seen in the SFG, as anticipated by the theoretical predictions (Figure 5). The weak symmetric and antisymmetric ketone modes exhibit little sensitivity to polarization. In contrast, the aromatic νCC mode and collective mode at 1350 cm⁻¹ have pronounced but different polarization dependencies. This would occur if the TDMs of these modes were oppositely aligned. The Gaussian software package⁴³ was used to calculate the TDMs and visualize their directions relative to the molecular axes. The insets in Figure 7 shows that the TDM for the strongest νCC mode is aligned with the minor axis of the PAH while a TDM for the collective ring mode is aligned with the major axis. Thus, the polarization dependence is consistent with an edge-on orientation. It is likely that the two ketone groups orient to be in contact with the water because the hydrophobic alkyl chains partially shield the ester groups whereas the ketones are exposed. An edge-on orientation is also the most likely configuration consistent with the MMA, and it explains why the νCC mode is enhanced in SSP while the collective mode is enhanced in SPS. A head-on geometry would show the opposite polarization dependence to what is observed.

The νCC modes and collective ring modes show intensity in both polarizations because there are several νCC and collective modes with different orientations. The νCC has two weak modes with TDMs aligned with the long axis and out of plane, respectively, which can explain the much weaker signal in SPS

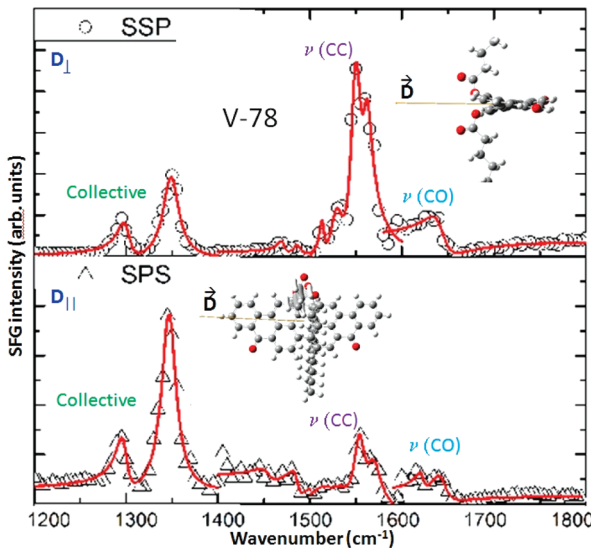


Figure 7. V-78: SFG spectra for a five layer V-78 LB film for SSP (top) and SPS (bottom) polarizations. Note the pronounced different polarization dependence of the aromatic $\nu(\text{CC})$ mode and collective modes. The two insets show a TDM for the $\nu(\text{CC})$ aligned with the minor axis of the molecule and a TDM for a collective mode aligned with the major axis.

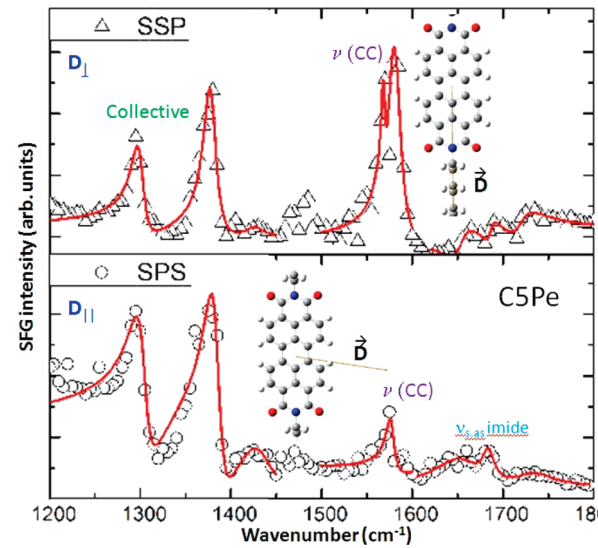


Figure 9. CSPe: SFG spectra for a five layer CSPe LB film for SSP (top) and SPS (bottom) polarizations. Note the pronounced different polarization dependence of the aromatic $\nu(\text{CC})$ mode and collective modes. The two insets show a TDM for the $\nu(\text{CC})$ aligned with the minor axis of the PAH and a TDM for a collective mode aligned with the major axis.

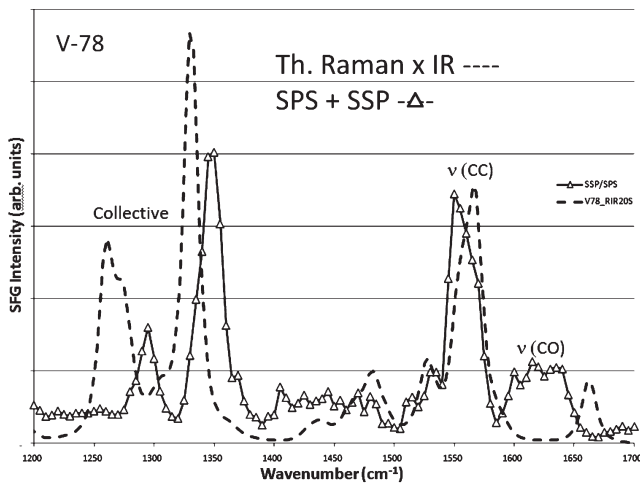


Figure 8. V-78: Comparison of the sum of the SSP and SPS SFG intensities with the product of the theoretical IR \times Raman intensities (RIR_{th}) for V-78. Apart from normalization of the relative intensities to the $\nu(\text{CC})$ mode and application of a correction factor as described in the text, no further manipulations have been performed.

polarization (for an edge-on geometry). Two out of three collective ring modes in the 1350 cm⁻¹ region are aligned with the long axis of the PAH; thus, this group is more strongly enhanced in SPS. However, we also cannot rule out that the intermolecular packing arrangement is such that the molecule is not 100% aligned with either the surface normal or the surface plane. In any case, there is no doubt that the V-78 adopts a perpendicular orientation rather than the flat-on geometry and shows a high degree of alignment.

In Figure 8, we compare the sum of the SSP and SPS SFG intensities with the RIR_{th} for V-78. Other than the correction factor (0.9614) and normalization, no other manipulations have been

carried out. The position of the $\nu(\text{CC})$ mode is quite accurately predicted by the calculation. The largest discrepancy lies with the position of the ketone, which is red-shifted by -35 cm^{-1} relative to the theory. When the molecule is transferred to the substrate during deposition, the ketones attach to the substrate and, consequently, exhibit a larger spectral shift than the collective modes which are shifted toward higher wavenumbers in the condensed phase.

Figure 9 shows the SFG spectra for a five layer CSPe LB film in SSP (top) and SPS (bottom) polarizations. The imide and carboxylic modes are weak in SFG due to a weak Raman signal (Figure 6). The carboxylic mode, which was not apparent in the ATR IR spectrum, is visible in the SFG. The aromatic $\nu(\text{CC})$ (1570 cm^{-1}) and collective ring modes (1270 and 1370 cm^{-1}) are the strongest modes in SFG. Similar to the V-78 molecule, the aromatic $\nu(\text{CC})$ modes and collective modes have pronounced but opposite polarization dependencies with the $\nu(\text{CC})$ being much stronger in SSP than in SPS. However, in contrast to V-78, the collective ring modes appear equally intense for both polarizations. The two insets in Figure 9 show a TDM for the $\nu(\text{CC})$ aligned with the major axis of the PAH and a TDM for a collective mode aligned with the minor axis. Since the SSP (SPS) polarization excites modes which have a TDM perpendicular (parallel) to the interface, the observation that the $\nu(\text{CC})$ mode is stronger in SSP than in SPS is fully consistent with the molecule adopting a head-on geometry, with the PAH core orientated perpendicular to the interface.

Some degree of polarization mixing could be attributed to an intermolecular packing arrangement in which the PAH core is not fully aligned with the surface normal but tilted at an angle. For the collective modes in the range 1270 – 1370 cm^{-1} , some TDMs are aligned with the short axis and some with the long axis of the PAH, and thus, the polarization sensitivity relative to the $\nu(\text{CC})$ is not as pronounced. An edge-on geometry should show an opposite polarization dependence to our observations because the TDMs of the strongest $\nu(\text{CC})$ modes are parallel to the major axis. It is more likely that the carboxylic acid is in contact with the

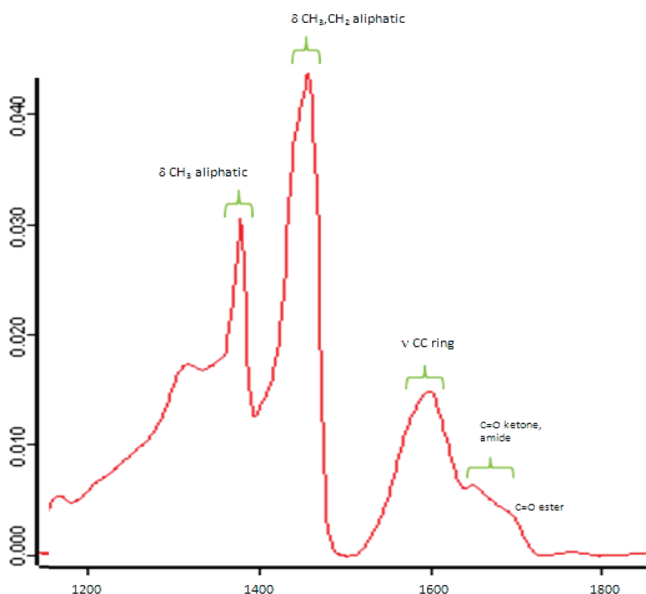


Figure 10. UG-8: Experimental FTIR-ATR powder spectra corresponding to the region probed by SFG. The carbonyl, $\nu(\text{CC})$ aromatic, and aliphatic deformation modes are identified in the figure.

water because it is more polar than the ketones. Thus, we believe that the head-on orientation is the most likely configuration consistent with both the MMA and SFG. Only a head-on geometry can explain both the enhanced signal from the νCC mode in SSP and the enhanced signal from the collective mode in SPS. In any case, there is no doubt that the C5Pe adopts a perpendicular orientation rather than flat-on geometry and shows a high degree of alignment.

Figure 10 shows a MIR-ATR powder spectrum of UG8 asphaltene with the modes labeled. Figure 11 shows SFG data in the same region for a LB asphaltene film. The δCH_2 and δCH_3 are enhanced in SSP polarization, and the νCC is enhanced in SPS. In contrast to the model compounds, the asphaltenes appear to be anisotropic, and fully molecularly aligned at the interface, because the aliphatic modes are not visible in SPS and aromatic is absent in SSP. Thus, the data show unambiguously that the asphaltene PAHs are parallel to the interface while the asphaltene alkanes are perpendicular to the interface.

In the model compounds, the polar or charged O moieties (C5Pe = 12.68%, V-78 = 9.4%) are in exposed and interfacially active sites. In contrast, the oxygen content of asphaltenes is generally low (UG8 = 1.6%), with acid groups present only in small concentrations. We speculate that other types of asphaltenes will orient similarly to UG8 because the variations in oxygen content that are typically observed are small and therefore are not likely to influence the alignment.

Sulfur is the predominant heteroatom; however, its species are less polar or charged in asphaltenes than either N or O and therefore less likely to play a significant role in molecular orientation. Small quantities of nitrogen are found in asphaltenes, all in pyrrole and pyridine type moieties;⁵⁰ consequently, there is some charge separation in the asphaltene PAH. However, for most asphaltene molecules, the aromatic core is the site of the greatest molecular polarizability. Moreover, it is the polarizability that gives rise to many of their properties.⁵¹ Thus, we believe it is the asphaltene ring system rather than the relative amount of heteroatoms which determines the alignment.

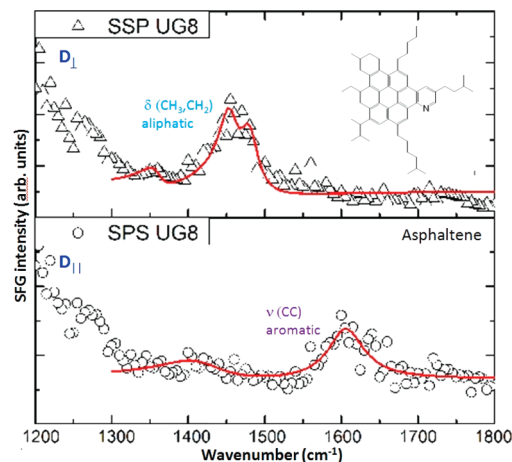


Figure 11. UG-8: SFG SSP (perpendicular) and SPS (parallel) intensities. The asphaltenes appear to be anisotropic and thus molecularly aligned at the interface. The data show unambiguously that the asphaltene PAHs are parallel to the interface while the asphaltene alkanes are perpendicular to the interface. The inset shows a hypothetical asphaltene structure.

It is not surprising that, without other strongly hydrophilic groups, the asphaltene PAH would align parallel with the interface. Moreover, it is expected and observed here by SFG that the asphaltene alkanes are perpendicular to the interface. This consistency builds confidence that indeed the interpretation of the SFG data regarding asphaltene PAHs is correct. Theoretical support for these observations is provided by recent molecular dynamics simulations of asphaltenes on a mineral surface.⁵²

We note that very low initial concentrations ($\sim 0.2 \text{ mg/mL}$) have been used to prepare the asphaltene film. The concentration is below the critical nanoaggregate concentration (CNAC), and thus, a molecular dispersion of asphaltene in the Langmuir film is expected. It is possible that during surface compression some aggregation occurs prior to LB deposition, consistent with the observed small MMA. Nevertheless, these nanoaggregates that could form by surface compression may have a molecular orientation memory of the initial molecular dispersion. The deposition process could also affect the orientation because the structure of the LB film at the water interface is transferred to the substrate. The asphaltenes are forced to the interface by toluene evaporation so that a bulk film is obtained, not only the most interfacially active moieties. Determining orientation versus concentration is likely a worthwhile future experiment.

4. CONCLUSIONS

The SFG results show that asphaltenes are highly oriented in Langmuir–Blodgett films with their PAH in plane and the alkyl groups out of plane. This result indicates that understanding asphaltene and petroleum interfacial science necessitates not only a molecular understanding of asphaltenes but in addition requires knowledge of molecular orientation, which SFG is uniquely positioned to provide. The measured orientation is consistent with the “island” asphaltene molecular architecture, with a single somewhat large PAH per asphaltene molecule. This may be required to yield highly oriented aromatic carbon, since small cross-linked PAHs would likely align less due to steric constraints. Thus, island architecture could yield the observed alignment, but our results do not prove the absence of archipelago structures since we

have not investigated these model compounds. Island model PAH compounds also exhibit a high degree of molecular orientation, consistent with the above reasoning. However, due to different functionality discussed below, the model compounds show different orientation from that of asphaltenes.

SFG clearly demonstrates that the asphaltenes adopt an orientation that is transverse to the model compounds, with the PAH core in parallel to the interface and the alkyl chains perpendicular to the interface, in sharp contrast to the model compounds for which the PAH core is aligned in an edge configuration. In contrast to asphaltenes, the model compounds examined here have oxygen functional groups. In addition, these functional groups are either on the alkyl chains or at the edges of the core. For asphaltenes, there is little oxygen functionality, and peripheral substituents are predominantly alkane. The asphaltenes also possess some polarity within the PAH due to nitrogen functionalities. These chemical structural differences plausibly give rise to the opposite orientation of various model compounds examined here versus asphaltenes. Future work involving SFG needs to investigate the role of asphaltene aggregation, and make use of atomically rough (mineral) surfaces associated with oil-bearing rock formations in order to connect basic science results herein with wettability impact on oil production. Nevertheless, these experiments represent a major step forward in treating important phenomenology of petroleum interfacial science from a first principles approach.

AUTHOR INFORMATION

Corresponding Author

*E-mail: bandrews@slb.com. Phone: +1 617 768 2154. Fax: +1 617.768.2398.

ACKNOWLEDGMENT

We would like to thank Prof. Mary Shultz (Tufts U.) for many discussions about SFG, Prof. Katarzyna M. Marzec (Jagiellonian U.) for calculations with an augmented basis set, and Dr. Sergey Shilov (Bruker Optics) for assistance with PM-IRRAS experiments.

REFERENCES

- (1) Sandrea, I.; Sandrea, R. *Oil Gas J.* **2007**, *105*, (42), 39–42.
- (2) Carnegie, A. Society of Petroleum Engineers, SPE# 99240, SPE/DOE Symposium on Improved Oil Recovery, Tulsa, Oklahoma, 2006; DOI: 10.2118/99240-MS.
- (3) Zhang, L. Y.; Lawrence, S.; Xu, Z.; Masliyah, J. H. *J. Colloid Interface Sci.* **2003**, *264*, 128–140.
- (4) Zhang, L. Y.; Lawrence, S.; Xu, Z.; Masliyah, J. H. *Ind. Eng. Chem. Res.* **2005**, *44*, 1160–1174.
- (5) Cadena-Nava, R. D.; Cosutchi, A.; Ruiz-Garcia, J. *Energy Fuels* **2007**, *21*, 2129–2137.
- (6) Lobato, M. D.; Pedrosa, J. M.; Hortal, A. R.; Martínez-Haya, B.; Lebón-Aguilar, R.; Lagoa, S. *Colloids Surf., A* **2007**, *298*, 72–79.
- (7) Lobato, M. D.; Pedrosa, J. M.; Möbius, D.; Lago, S. *Langmuir* **2009**, *25*, 1377–1384.
- (8) Orbulescu, J.; Mullins, O. C.; Leblanc, R. M. *Langmuir* **2010**, *26*, 15257–15264.
- (9) Orbulescu, J.; Mullins, O. C.; Leblanc, R. M. *Langmuir* **2010**, *26*, 15265–15271.
- (10) Nordgard, E. L.; Landsem, E.; Sjøblom, J. *Langmuir* **2008**, *24*, 8742–8751.
- (11) Sorland, G. *Langmuir* **2010**, *26*, 2352–2360.
- (12) Antunes, P. A.; Constantino, C. J. L.; Aroca, R. F.; Duff, J. *Langmuir* **2001**, *17*, 2958–2964.
- (13) Constantino, C. J. L.; Antunes, P. A.; Oliveira, C. B.; Trsic, M.; Caracelli, I.; Aroca, R. F. *Canadian J. Anal. Sci. and Spec.* **2004**, *49*, 64–72.
- (14) Wurthner, F.; Chen, Z.; Dehm, V.; Stepanenko, V. *Chem. Commun.* **2006**, 1188–1190.
- (15) Andreatta, G.; Bostrom, N.; Mullins, O. C. *Langmuir* **2005**, *21*, 272.
- (16) Mullins, O. C. *Energy Fuels* **2010**, *24*, 2179–2207.
- (17) Mullins, O. C. *The Asphaltenes. Annu. Rev. Anal. Chem.* **2011**, *4*, 393–418.
- (18) Zajac, G. W.; Sethi, N. K.; Joseph, J. T. *Scanning Microsc.* **1994**, *8*, 463.
- (19) Sharma, A.; Groenzin, H.; Tomita, A.; Mullins, O. C. *Energy Fuels* **2002**, *16*, 490.
- (20) Ruiz-Morales, Y.; Mullins, O. C. *Energy Fuels* **2009**, *23*, 1169–1177.
- (21) Boek, E. S.; Yakovlev, D. S.; Headen, T. F. *Energy Fuels* **2009**, *23*, 1209–1219.
- (22) Groenzin, H.; Mullins, O. C. *Energy Fuels* **2000**, *14*, 677.
- (23) Schneider, M. H.; Andrews, A. B.; Mitra-Kirtley, S.; Mullins, O. C. *Energy Fuels* **2007**, *21*, 2875–2882.
- (24) Andrews, A. B.; Guerra, R.; Mullins, O. C.; Sen, P. N. *J. Phys. Chem. A* **2006**, *110*, 8095.
- (25) McKenna, A.M.; Purcell, J. M.; Rodgers, R.P.; Marshall, A.G. 9th Int'l Conference on Petroleum Phase Behavior & Fouling, Victoria, B.C., Canada, Abstract #17, 2008.
- (26) Sabbah, H.; Morrow, A. L.; Pomerantz, A. E.; Zare, R. N. *Energy Fuels* **2011**, DOI: 10.1021/ef101522w.
- (27) Borton, D.; Pinkston, D. S.; Hurt, M. R.; Tan, X.; Azyat, K.; Scherer, A.; Tykwiński, R.; Gray, M.; Qian, K.; Kenttämäa, H.I. *Energy Fuels* **2010**, *24*, 5548–5559.
- (28) Andrews, A. B.; Edwards, J. C.; Pomerantz, D.; Mullins O. C.; and Norinaga, K. *Energy Fuels*, submitted.
- (29) Shen, Y. R. *Nature* **1989**, *337*, 519–525.
- (30) Wang, J.; Chen, C. Y.; Buck, S. M.; Chen, Z. *J. Phys. Chem. B* **2001**, *105*, 12118–12125.
- (31) Wang, J.; Woodcock, S. E.; Buck, S. M.; Chen, C. Y.; Chen, Z. *J. Am. Chem. Soc.* **2001**, *123*, 9470–9471.
- (32) Chen, C. Y.; Even, M. A.; Wang, J.; Chen, Z. *Macromolecules* **2002**, *35*, 9130–9135.
- (33) Walker, D. S.; Richmond, G. L. *J. Phys. Chem. C* **2008**, *112*, 201–209.
- (34) Richmond, G. L. *Annu. Rev. Phys. Chem.* **2001**, *52*, 357–89.
- (35) Chen, Z.; Shen, Y. R.; Samorjai, G. A. *Annu. Rev. Phys. Chem.* **2002**, *53*, 437–465.
- (36) Richmond, G. L. *Chem. Rev.* **2002**, *102*, 2693–2724.
- (37) Shultz, M. J. *Advances in Multi-photon Processes and Spectroscopy*; Lin, S. H., Villaey, A. A. Fujimura, Y., Eds.; World Scientific: Singapore, Japan, 2008; Vol. 18, pp 133–200.
- (38) Gopalakrishnan, S.; Liu, D.; Allen, H. C.; Kuo, M.; Shultz, M. J. *Chem. Rev.* **2006**, *106*, 1155–1175.
- (39) Langmuir, I. *J. Am. Chem. Soc.* **1917**, *39*, 1848.
- (40) Blodgett, K. A. *J. Am. Chem. Soc.* **1935**, *57*, 1007.
- (41) Peterson, I. R. *Langmuir Blodgett Films. J. Phys. D* **1990**, *23*, 379–95.
- (42) Petty, C. P. *Langmuir-Blodgett Films: An Introduction*; Cambridge University Press: Cambridge, UK, 1996.
- (43) Frisch, M. J.; Trucks, G. W.; Schlegel, H. B.; Scuseria, G. E.; Robb, M. A.; Cheeseman, J. R.; Montgomery, J. A., Jr.; Vreven, T.; Kudin, K. N.; Burant, J. C.; Millam, J. M.; Iyengar, S. S.; Tomasi, J.; Barone, V.; Mennucci, B.; Cossi, M.; Scalmani, G.; Rega, N.; Petersson, G. A.; Nakatsuji, H.; Hada, M.; Ehara, M.; Toyota, K.; Fukuda, R.; Hasegawa, J.; Ishida, M.; Nakajima, T.; Honda, Y.; Kitao, O.; Nakai, H.; Klene, M.; Li, X.; Knox, J. E.; Hratchian, H. P.; Cross, J. B.; Bakken, V.; Adamo, C.; Jaramillo, J.; Gomperts, R.; Stratmann, R. E.; Yazyev, O.; Austin, A. J.; Cammi, R.; Pomelli, C.; Ochterski, J. W.; Ayala, P. Y.; Morokuma, K.; Voth, G. A.; Salvador, P.; Dannenberg, J. J.; Zakrzewski, V. G.; Dapprich, S.; Daniels, A. D.; Strain, M. C.; Farkas, O.; Malick, D. K.; Rabuck, A. D.; Raghavachari, K.; Foresman, J. B.; Ortiz, J. V.; Cui,

Q.; Baboul, A. G.; Clifford, S.; Cioslowski, J.; Stefanov, B. B.; Liu, G.; Liashenko, A.; Piskorz, P.; Komaromi, I.; Martin, R. L.; Fox, D. J.; Keith, T.; M. A. Al-Laham, Peng, C. Y.; Nanayakkara, A.; Challacombe, M.; Gill, P. M. W.; Johnson, B.; Chen, W.; Wong, M. W.; Gonzalez, C.; , Pople, J. A. *Gaussian 03*, revision D.01; Gaussian, Inc.: Wallingford, CT, 2004.

- (44) Becke, A. D. *J. Chem. Phys.* **1993**, *98*, 5648.
- (45) Lee, C.; Yang, W.; Parr, R. G. *Phys. Rev. B* **1988**, *37*, 785.
- (46) Ditchfield, R.; Hehre, W. J.; Pople, J. A. *J. Chem. Phys.* **1971**, *54*, 724.
- (47) Hehre, W. J.; Ditchfield, R.; Pople, J. A. *J. Chem. Phys.* **1972**, *56*, 2257.
- (48) Hariharan, P. C.; Pople, J. A. *Theor. Chim. Acta* **1973**, *28*, 213.
- (49) Scott, A. P.; Radom, L. *J. Phys. Chem.* **1996**, *100*, 16502.
- (50) Mitra-Kirtley, S.; Mullins, O. C.; Chen, J.; van Elp, J.; George, S. J.; Cramer, S. P. *J. Am. Chem. Soc.* **1993**, *115*, 252.
- (51) Buckley, J. S.; Wang, J.; Creek, J. L. In *Asphaltenes, Heavy Oils and Petroleomics*; Mullins, O. C., Sheu, E. Y., Hammami, A., Marshall, A. G., Eds.; Springer: New York, 2007; Chapter 16.
- (52) Headen, T. F.; Boek, E. S. *Energy Fuels* **2011**, *25*, 499–502.